Advances in Geo-Energy Research

Adv. Geo-Energy Res. Vol. 1, No. 1, p. 18-30, 2017
Ausasia Science and Technology Press

Invited review

Applications of digital core analysis and hydraulic flow units in petrophysical characterization

Xiaojun Chen[1]*, Yingfang Zhou[2]

[1]*Faculty of Earth Resources, China University of Geosciences, Wuhan 430074, P. R. China*

[2]*School of Engineering, University of Aberdeen, Aberdeen, AB24 3UE, The UK*

(Received March 12, 2017; revised April 15, 2017; accepted April 18, 2017; published June 25, 2017)

Abstract: Conventional petrophysical characterizations are often based on direct laboratory measurements. Although they provide accurate results, such measurements are time-consuming and limited by instrument and environment. What's more, in the geo-resource energy industry, availability and cuttings of core plugs are difficult. Because of these reasons, virtual digital core technology is of increasing interest due to its capability of characterizing rock samples without physical cores and experiments. Virtual digital core technology, also known as digital rock physics, is used to discover, understand and model relationships between material, fluid composition, rock microstructure and macro equivalent physical properties. Based on actual geological conditions, modern mathematical methods and imaging technology, the digital model of the core or porous media is created to carry out physical field numerical simulation. In this review, the methods for constructing digital porous media are introduced first, then the characterization of thin rock cross section and the capillary pressure curve using scanning electron microscope image under mixed wetting are presented. Finally, we summarize the hydraulic flow unit methods in petrophysical classification.

Keywords: Digital core, porous media, petrophysical characterization, thin section, mercury injection capillary pressure.

Citation: Chen, X., Zhou, Y. Applications of digital core analysis and hydraulic flow units in petrophysical characterization. *Adv. Geo-Energy Res.* 2017, 1(1): 18-30, doi: 10.26804/ager.2017.01.02.

1. Introduction

In the past decades, significant advances in both microscopic imaging and computational power have been made, which helped to develop digital rock physics (DRP) into a new technology to study petrophysical properties (e.g., elastic, transport, and electrical properties) of rocks and porous media in various materials. For deeper understanding of visualization of pore structure, mineral composition with their spatial arrangement, and relevant physical processes are used in combination with the dataset captured by DRP technique for advanced numerical simulations. DRP has been effectively used for earth, material and soil-science related problems. Three steps are included primarily in the DRP workflow: 1) digitally imaging, such as μxCT (Table 1), scanning electron microscope (SEM) and thin section for multi-scale pores and solids different resolution; 2) image (gray-scale or RGB colored) processing, such as segment pore from the mineral matrix phases; and 3) simulating processes and calculating the petrophysical parameters, such as electricalconductivity, permeability, capillary pressure curve, relative permeability curve, porosity, mineral identification, rock type, elastic modulus, molecular dynamics-based diffusion etc. A crucial workflow and associated computational method was summarized by Liu et al. (2016a) (Fig. 1).

Further, due to blurred boundaries among pore-solid or materials, manual segmentation according to visual observation is usually not feasible. Instead, an automatically algorithm that couples manual interaction and quality control is required to perform the task of spatial filtering, de-noising, thresholding, boundary extraction, distance transformation and cluster analysis for a grayscale image. An excellent review of image segmentation methods applied to pore-solid structure analysis for porous media is given by Sezgin (2004) and Iassonov et al. (2009). Alternatively, the 3D special model could be reconstructed statistically using 2D rock image, which normally are relatively easier to obtain; this process also known as 2D-to-3D rock image reconstruction (Liang et al., 2000; Keehm et al., 2004). The key to this technology is the use of similar microstructural properties between 2D images and

*Corresponding author. E-mail: chenxiaojuncug@hotmail.com

Table 1. CT imaging at multiscales under different resolutions (from irock technologies co., LTD).

CT scale	Specific rock size	Resolution	Purpose
Whole core scan	1 m long; 10 cm diameter	0.5 mm	Density logging; Core plug selection
Plug scan	Standard 1- or 1.15-in. plugs [2.5 mm or 38 mm across]	12 or 17 μm	Geological description; Heterogeneity study
Chip scan	1 cm long; 1 to 25 mm diameter	0.5 to 12 μm	Detailed scan and pore network analysis
Nano scan	Less than 1 mm	3 to 150 nm	Extreme samples: Shale, micrite, carbonate, tight gas, etc.

3D structures, such as porosity, two-point spatial correction function and linear path function. However, the application of 2D-to-3D reconstruction method is limited because it fails to accurately capture the real complex structure in terms of its pore connectivity and shapes. Considering the time consuming and expensive exercise of acquiring 3D microstructures, conceptual digital rock models have been developed using random algorithm, such as discrete element, quartet structure generation set (QSGS) and random packed sphere or sand bed structure. Based on these ideal numerical models, the relationship between variable microstructure parameters and petrophysical property can be explored quantitatively to overcome the limitations of natural samples in diversity. Additionally, 2D thin section is another alternative to study rock physics by using the information about pore, mineral and grain structure without reconstruction (Saxena and Mavk, 2016; Saxena et al., 2017).

Simulating physical processes need advanced numerical methods (Andrä et al., 2013), such as the Lippmann-Schwinger method (Wiegmann, 2007), the finite-element method (FEM) (Garboczi and Berryman, 2001; Khoei et al., 2016), the finite-difference method (FDM) (Zhan et al., 2010), lattice-Boltzmann method (LBM) (Shan and Chen, 1993; Li et al., 2016; Wang et al., 2016a), and the Explicit Jump method (EJ) (Wiegmann and Bube, 2000). For instance, recently a capillary pressure curve was simulated through minimum energy algorithm (Helland et al., 2013; Zhou et al., 2014; Zhou et al., 2015). However, some of the computational challenges include big data from micro-tomography, intensive computations of petrophysics and upscaling. A detail description of the challenges was presented by Liu et al. (2016a), including characterization of microstructures, determination of the representative volume element (RVE) and critical exponents for upscaling, accuracy of the method and cost of computing resources.

As the reservoir rocks have different physical phases in space, classification analysis is particularly important. Classification of petrophysical properties is an important part of oil and gas reservoirs, which includes estimation of permeability based on well-logging data, estimation of effective thickness and "sweet spot" in the reservoir, and estimation of remaining oil zone. In the final section, we also introduced the physical division of the rock based on the hydraulic flow units.

2. Imaging and construction of porous media

Imaging and construction of porous media is becoming a routine service in the geo-resource energy industry (Ismail et al., 2005), which can be divided into two steps: image generation, where the properties and details of porous media are extracted from the image (Hildebrand and Ruegsegger, 1997); and model construction, where the fluid flow and mass or sound waves transport are simulated through the constructed models of the porous media (Martys and Chen, 1996).

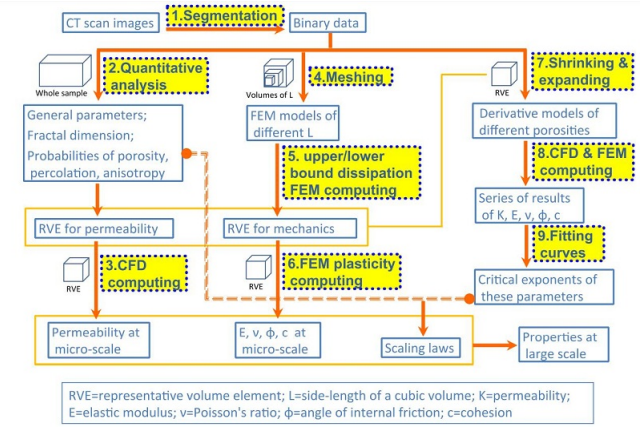

Fig. 1. Detailed workflow of analyzing and upscaling petrophysical properties from micro-tomography by Liu et al. (2016a).

At present, the state of the art method in capturing the 3D real and complex porous structure is computed tomography scanning using X-ray transmission through sample under high-precision positioning and rotation conditions (Blunt et al., 2013). The pore, fluid and solid are identified by the degree of attenuation of the transmitted X-ray (Arns et al., 2007). Fig. 2 shows 2D cross-sections of 3D images. Figs. 3(a) and 3(b) show the 3D images (Chen et al., 2017).

Besides the 3D reconstruction using 3D images, there are other methods that have been used in producing fine-scale images of rock samples. For high resolution requirements, FIB/SEM-first use FIB (focused ion beams) to make very fine slices through the samples (typically just a few μm across), that enable sequential SEM images to be obtained down to resolutions of 10 nm (Tomutsa et al., 2007; Lemmens et al., 2010).

The most popular approach for model construction is the network model. The first network model was constructed by Fatt (1956), who exploited the analogy between flow in porous media and a random resistor network. The widely-used maximal ball approach was developed to construct network model, where spheres are grown in the pore space, centered on each void voxel. The largest spheres represent pores, while chains of smaller spheres connecting them define throats (Silin

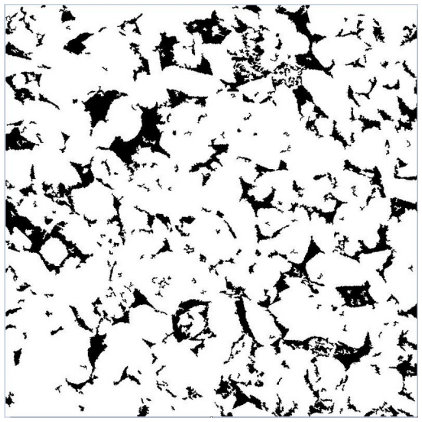

(a) M-1

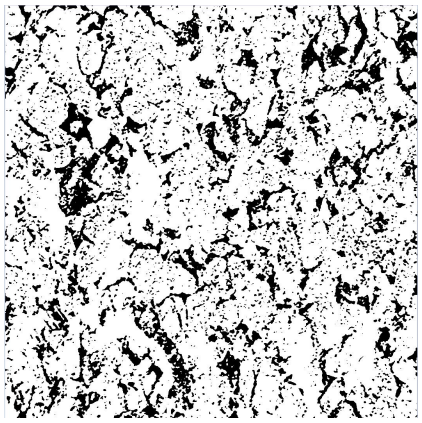

(b) M-66

Fig. 2. The μxCT images of rock samples which are gotten from Yinggehai basin, south of China (Chen et al., 2017). White and black pixels represent solid and pore respectively.

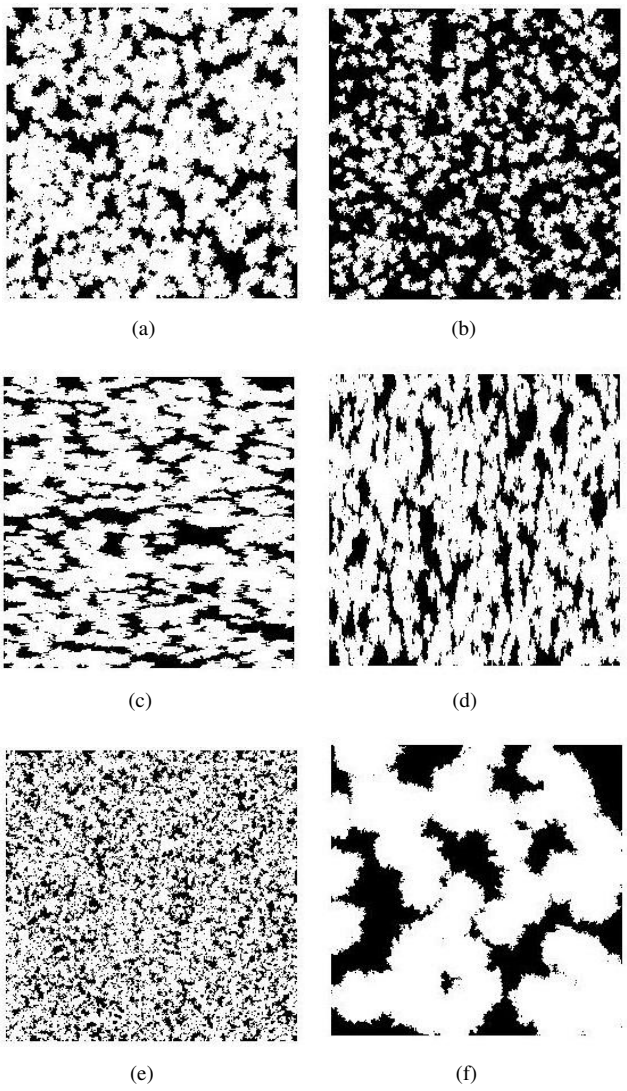

(a) (b) (c) (d) (e) (f)

Fig. 4. Porous media generated by RGG. (a) and (b) shows the difference of porosity. $\phi_a = 0.3$, $\phi_b = 0.6$. (c) and (d) shows the difference of anisotropy. (e) and (f) show the difference of heterogeneity. $\phi_{c-f} = 0.3$.

and Patzek, 2006; Dong and Blunt, 2009). Fig. 3(c) shows networks extracted from the pore space images shown in Fig. 3(a), by using the maximal ball approach.

Based on either the 3D image or pore network model, fluid flow simulations can be performed that can account for irregular lattices, wetting layer flow, arbitrary wettability, any sequence of displacement in two-and three-phase flow, phase exchange, non-Newtonian displacement, non-Darcy flow as well as reactive transport (Blunt et al., 2002; Lopez et al., 2003; Yiotis et al., 2006; Balhoff and Wheeler, 2009; Ryazanov et al., 2009).

It is well known that no two porous media have identical microstructure at all scales. Therefore, structure of porous media show high degree of randomness (Wolfram, 2002) and heterogeneity (Pan, 1994; Young et al., 2001). Developing whole complex structure of the field-scale porous medium is complex and technically impossible (Meakin, 1998); however, for this and other practical reasons it is not required to construct whole model at fine scale detail as some part of the porous media structureat fine scale may not affect the overall physical properties of porous media.

In regards to above discussions, some studies have conducted for the porous media reconstruction. For instance, Wang et al. (2007) proposed a multi-parameter random generation-growth (RGG) method to reproduce the random and multiphase microstructures using given statistical information from images and using the lattice Boltzmann method (Chen and Doolen, 1998; Raabe, 2004) to calculate the transport properties on the RGG model, which agree well with the properties of porous media (Wang and Pan, 2008). The RGG model has another advantage that it can be adjusted to some structural properties, such as porosity, anisotropy, heterogeneity. Thus, transport properties can be predicted at multi-scale and for variable properties of core, which cannot be done from a single physical core obtained from the subsurface.

Therefore, physically it is important to reconstructing a representative porous medium with identical petrophysical properties as that measured from core, and DRP make it possible from a modeling perspective.

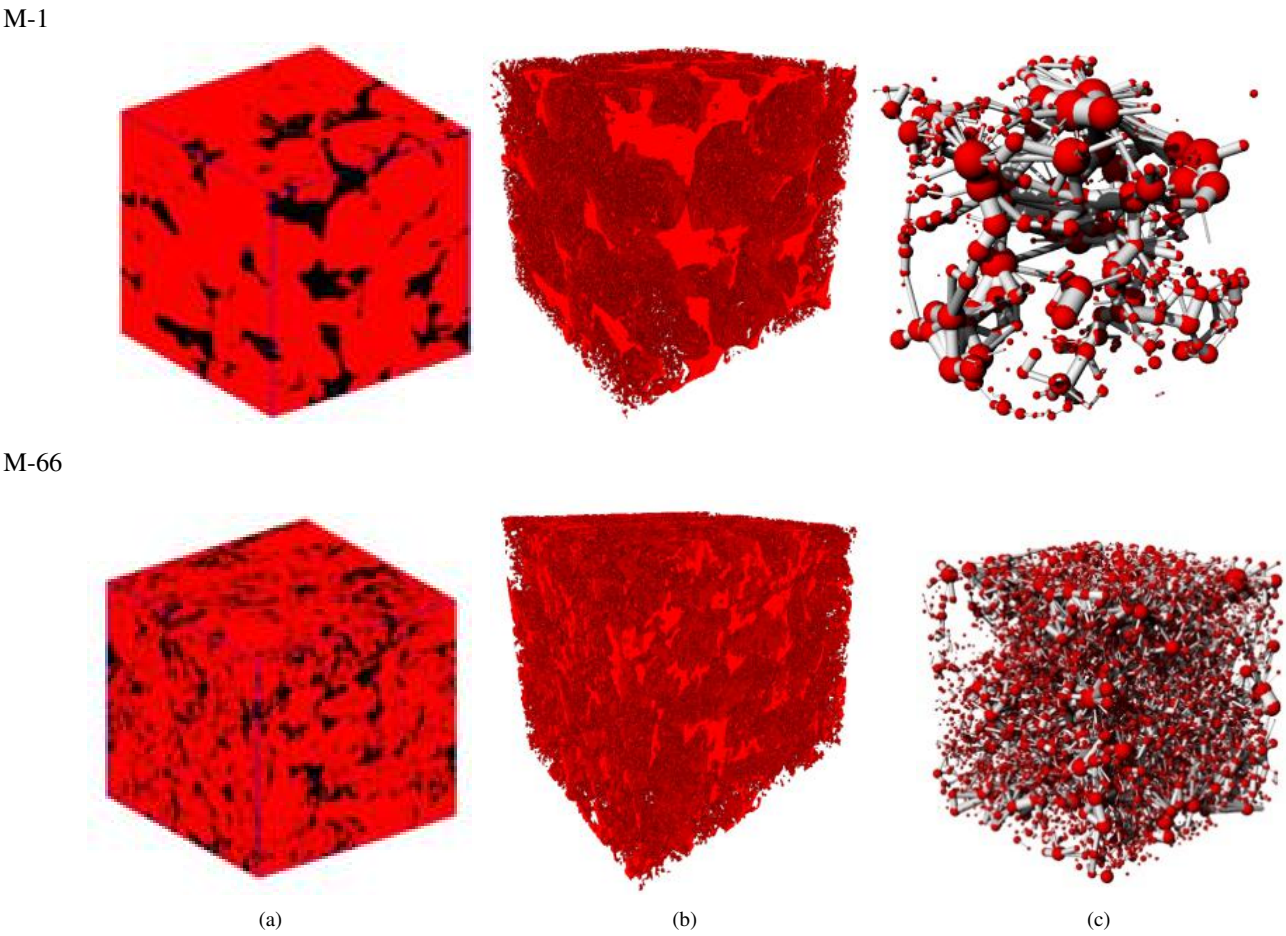

Fig. 3. (a) The μxCT thin sections of samples in three directions; (a) black part represents the pore phase, (b) the pore in space arrangement, and (c) the pore networks, in which red spheres represent pores and silver white rods represent throat, generated using maximum ball (MB) algorithm, for different hydraulic flow unit with the volume of 500^3 pixels (0.4753 in mm).

3. Petrophysical characterization based on thin section analysis

SEM can achieve relative high resolution in imaging pore-morphology, but with limited field of view and thus it may not fully and integrally reflect the overall pore distribution. X-ray CT can achieve wider field of view and very high resolution in 3D space (Ge et al., 2015). Despite the lower resolution in comparison with μxCT and SEM images, the thin section images have other advantages such as a wider range of view, saved time and cheaper availability for petrophysical studies, such as pore microstructure (Desbois et al., 2011; Rabbani et al., 2014a; Borazjani et al., 2016; Gundogar et al., 2016; Rabbani et al., 2016; Xiao et al., 2016), mineral recognition and classification (Hofmann et al., 2013; Asmussen et al., 2015; Izadi et al., 2015; Izadi et al., 2017b), specific surface area (Rabbani and Jamshidi, 2014; Rabbani et al., 2014b), elastic modulus (Arns et al., 2002; Dvorkin et al., 2011; Madonna et al., 2012; Saxena and Mavko, 2016), rock type determination (Mynarczuk, 2010; Mynarczuk et al., 2013; Ge et al., 2015; Mollajan et al., 2016), pore-grain analysis (Rabbani and Jamshidi, 2014; Rabbani et al., 2014b; Song et al., 2016), flowing property (Peng et al., 2016; Wang et al., 2016b). Using thin section images, the interconnected pore structure can be marked out visually as they are filled by color epoxy resin. As presented in Fig. 5, the pore structure in the granular limestone from the cross thin section, where the pore space is marked with blue plexiglass. Pore-solid segmentation work based on digital image analysis (DIA) is particularly important in petrographic, soil science and porous material research, and it is the premise and basis for calculating the number, size distribution and boundary of pores (or grains).

With the rapid rise of DIA techniques, precise pore area can be presented from the binary image using various segmentation methods such as Otsu method (Otsu, 1975), Kriging method (Otsu, 1975), Kriging method (Oh and Lindquist, 1999; Houston et al., 2013a), and K-mean clustering method (Izadi et al., 2015; Aliyev et al., 2016). This is done typically by reading an image through some software as a matrix consisting of binary elements with the size m*n. The binary image data matrix A [m×n] has values 0 and 1, where 0 represents white and 1 is the black respectively. Using this matrix, the porosity is calculated as:

$$\phi = \frac{\sum N}{mn} \tag{1}$$

where N is the total number of pore pixels (white area). The pore-throats distribution plays a leading role in porous rock.

The specific information about the pore patterns and arrangement in the 2D plane is analogous to the 3D context. In order to obtain spatial structural information to flow simulation, two-point correlation function (e.g., variogram or covariance) or multiple-point statistics algorithms were developed for pore space reconstruction from geometrical properties in 2D images (Okabe and Blunt, 2005; Hajizadeh et al., 2011; Comunian et al., 2012; Xu et al., 2012; Izadi et al., 2017a). In addition to the pore structure, the distribution of pores and solid particles also affects the rocks transport capacity. Pure sandstone formed by larger-size grain has larger permeability and porosity (Vidal et al., 2009; Byon and Kim, 2013; Wang et al., 2016b). Size, distribution, and contact relationship of pores and solids or grains are clearly displayed in thin section. Since scattered pore area and solids in contact and extrusion with each other, it is difficult to count and measure the size of a single pore or solid. Watershed algorithm based on distance transform is a powerful tool that is used for segmentation and classification of attached clusters of objects (Malpica et al., 1997; Rabbani et al., 2014a). Four different forms of distances were discussed by Rabbani et al. (2014a). The results showed that city-block and chessboard distance have explicit change and separate in best results. Their work also proposed a simple method to compute average diameter using test lines scanning:

$$\bar{d} = \frac{4}{\pi}\frac{M}{m}\sum_{i=1}^{m}\left\langle d_i \right\rangle \tag{2}$$

where $\langle d_i \rangle$ is the averaged length of the solid lines in the ith row in Fig. 6; m is the total number of solid lines, less than or equal to the width or height size of the image in pixels, and M is the resolution of the image corresponding to the actual length of each pixel. Conversely, the average diameter of the pores can be obtained. After obtaining the data set on the number and size of the pores or particles, another important geological parameter specific surface, S, can be evaluated using Eq. (3),

$$S = \frac{Specific\ area\ of\ grains}{Volume\ of\ rock\ grains} \tag{3}$$

However, in 2D thin section, the volume of corresponding 3D space is not available. Thus, the parameter specific perimeter, P_s, is more suitable, which is defined as:

$$P_s = \frac{Object\ Perimeter}{Object\ surface\ area} \tag{4}$$

Previous work showed that P_s and S can be correlated by $S = 1.35\ P_s$ (Rabbani et al., 2014b).

Thin sections are the RGB images with the pore area marked by colored epoxy resin. They also express mineral characteristics in addition to the rich pore-solid information (see Fig. 7). Mineral analysis in oil and gas reservoir also plays an important role in the depositional environment, source direction, mechanical properties and development program. Different minerals have different optical properties. By single polarization and orthogonal polarization, diagenetic minerals showing different colors can be distinguished in the optical thin section.

RGB image color is a combination of three primary colors, red (R), green (G), blue (B). Thus, the data read from the RGB image is a 3D matrix $A = m \times n \times 3$, in which "3"represents the three-channel component of R, G, B respectively in each pixel (Eq. (5)) which ranges from 0 to 255.

$$A = \{x_i, y_j, R, G, B\}; (i = 1, 2, 3 \ldots m; j = 1, 2, 3 \ldots n) \tag{5}$$

where, x_i, y_j is the coordinate position of the pixel in the 2D plane, the origin (0, 0) at the upper left corner; $m \times n$ is the pixel size; i, j represents the position variable in the horizontal and vertical directions of the image. Therefore, it is possible to extract the region having the same color value, hence, the same mineral by using the DIA technology.

Each kind of mineral color is similar, and the boundary is blurred. Many algorithms were developed to classify and identify minerals, such as Seed Region Growing (SRG) (Asmussen et al., 2015), Artificial Neural Network (ANN) (Thompson et al., 2001; Marmo et al., 2005; Singh et al., 2010), genetic programming (GP) (Ross et al., 2001), color edge detection (Van den Berg et al., 2002). Recently, a novel method and an intelligent system for minerals segmentation were proposed by Izadi et al. (2015), in which clustering method and ANN were used without inputting the number of clusters in advance. A detailed procedure about the algorithm is shown in Fig. 8.

The exact characterization of the permeability is a challenging and important topic, with an active ongoing research in reservoir geology. Generally, reservoir rocks have low porosity ($< 35\%$), resulting in the non-connected pore areas between two sides in 2D thin cross sections. Thus, it is physically unrealistic to run flow simulations in them. Recently, the methodology to reconstruct pore network based on 2D thin section was developed for conventional sandstone reservoir using constant coordination number and stereological correction factor (Baveye et al., 2010; Houston et al., 2013a). For carbonate rock, which is a multiple porosity system, a fast but reliable method was proposed by Peng et al. (2016), through the relationship of K_{2D} (estimated by thin section) and K_{3D} (obtained by micro-CT scan and simulation) that are defined as:

$$K_{2D} = \frac{\phi_{2D} r_{h\_2D}^2}{\beta_{2D}} \tag{6}$$

$$K_{3D} = \frac{\phi_{3D} r_{h\_3D}^2}{\beta_{3D} \tau^2} \tag{7}$$

where β is a shape factor; subscript 2D and 3D represent the data acquisition from the 2D thin section and 3D μxCT. For complex 3D core sample, fractal theory is gaining increasing importance as a powerful tool in characterizing the pore structure, flow and transport (Cai et al., 2014b; Cai et al., 2015; Liu et al., 2015; Behrang and Kantzas, 2017). With the advancement in computational speed and power, it is expected that more developments in correlating thin slices with 3D space will be explored and discussed, especially in pore similarity, pore reconstruction and simple acquisition of flow performance.

4. Pore type and HFUs

Due to difference in sediments and late diagenetic processes, reservoir rock has a strong heterogeneity, rather than a uniform and layered cake, within and between different formations. Specifically, the simple Karman-Cozeny (K-C) equation is only applicable for some sandstone grains that exhibit reasonable homogeneous behavior, while there is no universal relationship between the pore and permeability that is applicable to all rocks. Permeability and porosity exhibit some direct correlation that can be used to estimate permeability from porosity data ideally, however, such site specific relationship has less correlation in the case of carbonate reservoirs. The pore space in the hydrocarbon-bearing strata has dramatic changes, complex arrangement and high anisotropy. When the reservoir enters the high water cut period, the remaining oil which is dominated by the difference of displacement efficiency within strata and flow characteristics, the sweep efficiency is highly affected by local heterogeneities and high channelized features. Therefore, for secondary or tertiary recover it is useful to develop refined sub-lithofacies or rock type to analyze pore structure and flow property to develop remaining resources and improve log-based interpretation accuracy of permeability for enhanced oil recovery. As early as 1950, a rock type was defined as units or volumes of rock deposited under similar diagenetic processes with a unique porosity-permeability relationship (Archie, 1950). Subsequently, another concept related to Hydraulic Flow Units (HFUs) was proposed (Yan et al., 2011; Sachsenhofer and Koltun, 2012; Clarkson et al., 2013; Wilson et al., 2016), which was defined as the minimum units in reservoir and the volume of rocks with similar petrophysical character that affects fluid flow, and classified by Sedimentary Microfacies Zonations (SMZ). SMZ technique has many limitations in the quantitative division in the vertical and flame due to the fuzzy microphase bound (Hinai et al., 2014). First quantitative method was proposed by Amaefule et al. (1993), using the parameters Flow Zone Indicator (FZI) and Reservoir Quality Indicators (RQI) derived from the modified Kozeny-Carmann (K-C) equation:

$$K = \frac{1}{F_s \tau S_g^2} \frac{\phi^3}{(1-\phi)^2} \tag{8}$$

where F_s the shape factor. ϕ is the effective porosity in fraction. S_g is the specific surface area of the grains. Taken the logarithm on both sides, Eq. (8) can be rearranged as:

$$\log \sqrt{\frac{K}{\phi}} = \log \frac{1}{\sqrt{F_s \tau} S_g} + \log \frac{\phi}{1-\phi} \tag{9}$$

in which $\sqrt{K/\phi}$ is defined as RQI, $\phi/(1-\phi)$ is defined as the normalized porosity ϕ_z, and $1/(\sqrt{F_s \tau} S_g)$ is defined as FZI, a structural parameter. From Eq. (8), in a log-log scatter plot of RQI versus ϕ_z, all samples with the same pore structure and capillary pressure profile, will have a same FZI value and yield a unique line with the slope 1, hence, constitute a HFU.

Actually, geological heterogeneity result in the scattered points of porosity vs. permeability. A HFU corresponds to a distribution around its mean value, which is difficult to classify

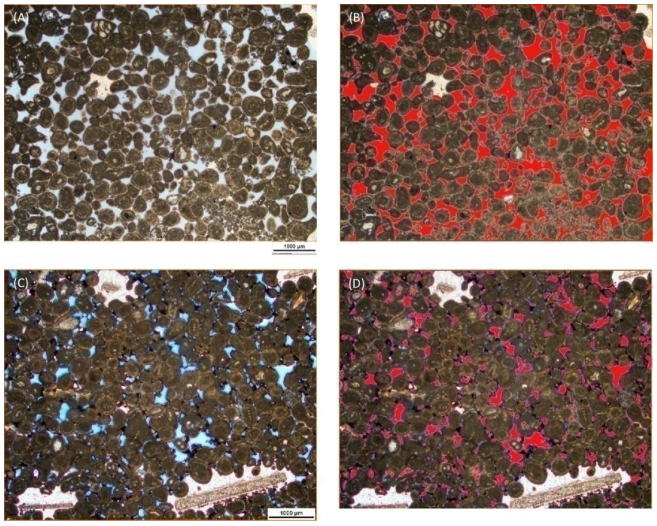

Fig. 5. Grainstone samples selected from Lower Cretaceous Thamama Group, Abu Dhabi Fields, with well-defined interparticle pores and minor cementation. Measured permeability is 2.0 D and 117.2 mD, respectively. (A) and (C) are cross thin sections; (B) and (D) are results of pore segmentation from (A) and (C). The original data are derived from Peng et al. (2016).

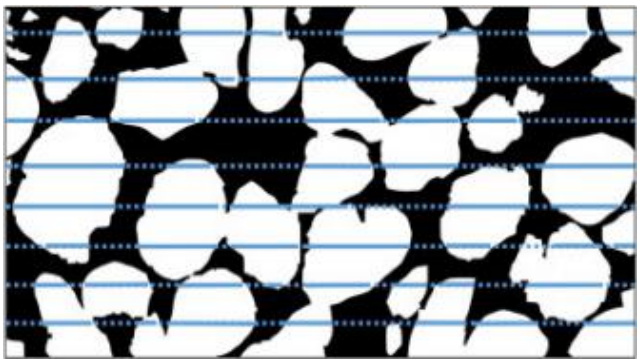

Fig. 6. Illustration of test lines scanning method used to estimate the average grain size from the binary image obtained by thin section, where the solid lines parts in the blue test line represent the grains. The original data are derived from Rabbani and Jamshidi (2014).

by several parallel lines. Cluster analysis techniques based on ANN were introduced to classify the point group of FZI according to the similarity (Clarkson et al., 2016). Recently, a committee fuzzy inference system based on genetic algorithm-pattern search technique and clustering technique using multi-resolution graph were developed for improving the accuracy of flow units prediction (Ougier-Simonin et al., 2016; Sander et al., 2017). The effects of distance function and linkage function on cluster results were discussed in detail.

The classical K-C equation has inherent limitations in estimating permeability because of with the porous media made up of capillary tubes is assumed to have fixed cross-sectional area (Yu and Cheng, 2002; Xu and Yu, 2008; Cai et al., 2010; Chalmers et al., 2012; Asmussen et al., 2015; Naraghi and Javadpour, 2015; Mollajan et al., 2016; Verma and Pitchumani, 2017). Thus, improved methods based on the modified K-C equation were proposed considering tortuosity term in a more robust manner (Peng et al., 2015), irreducible (or connate) water saturation with capillary trapping (Izadi et

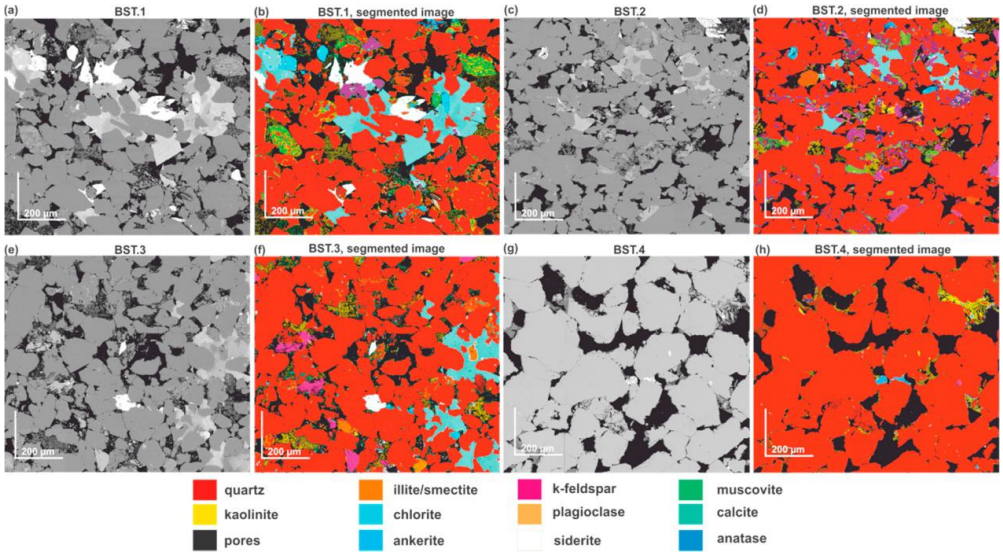

Fig. 7. Thin sections from four Berea sandstone core plugs (Cleveland Quarries, USA), Pore structure (a,c,e,g)and mineral information(b,d,f,h). the experiment were conducted by Kareem et al. (2017).

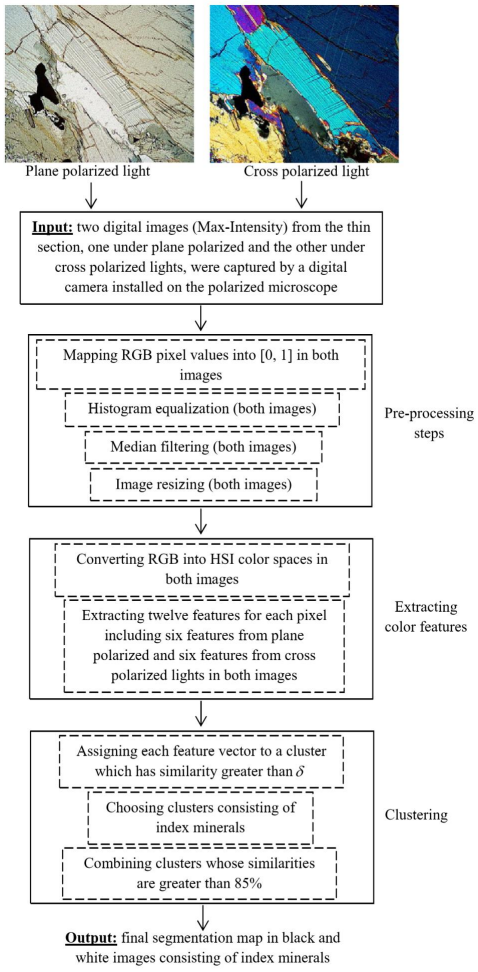

Fig. 8. Workflow proposed by Izadi et al. (2015) for intelligent mineral segmentation. After inputting data, pre-processing and color feature extraction steps, several black and white images in which show the index minerals are output.

al., 2017b) and mean hydraulic radius concept (Izadi et al., 2015) (see Table 2).

Furthermore, Stratigraphic Modified Lorenz Plot (SMLP) uses HFUs zonations in single well vertically (Ge et al., 2015; Zhao et al., 2017), in which the cumulative flow capacity (Kh) and the cumulative storage capacity ($K\phi$) are plotted. Inflection points in SMLP plot indicates changes in flow characteristics, hence the segment points of HFUs. Parts with high slope indicate faster rates of flow, hence high-quality HFUs or fast (reservoir) zones. This method can determine the number of HFUs in Vertical short-range well by well-log or experiments. Moreover, it is well known that pore throat aperture radii is a dominant factor in affecting flow (Houston et al., 2013b). Chen et al. (2017) analyzed the difference in pore structure of each HFUs based on the fractal theory. Winland r_{35} (pore radii at 35% mercury situation during MICP) is use to characterize the HFUs (Nie et al., 2015; Hikosaka et al., 2016; Fu et al., 2017) which can be estimated by the following empirical equation:

$$\log r_{35} = 0.732 + 0.588 \log K - 0.864 \log(100\phi) \qquad (10)$$

As reviewed by Mirzaei-Paiaman and Saboorian-Jooybari (2016) and Deng et al. (2016), among various methods, FZI or the modified FZI method is considered as the most effective and widely-used method for classifing HFUs for various types of reservoirs, such as sandstone (Wargo et al., 2013), tight gas (Xie et al., 2010; Aguilera, 2014), carbonate (Wang et al., 2011; Yang et al., 2017) and shale (Aguilera, 2010; Nie et al., 2015; Deng et al., 2016).

5. Capillary pressure curves from pore-scale modeling

The capillary pressure/saturation relationship (capillary pressure curve) is an important constitutive relationship in complex 3D porous structures for characterizing the transmission of fluid and mass, since it controls the fluids dis-

Table 2. Summary for the current improved methods based on the K-C equation for HFUs determination established by Hinai et al. (2014).

Reference	FZI or the modified	RQI or the modified	ϕ_Z or the modified
Nooruddin and Hossain (2011)	$\frac{1}{\sqrt{F_s}aS_g}$	$0.0314\sqrt{\frac{K}{\phi}}$	$\frac{\phi^m}{1-\phi}$
Izadi and Ghalambor (2013)	$\frac{1}{\sqrt{F_s}\tau S_g}$	$0.0314\sqrt{\frac{K}{\phi}}\sqrt{1-S_{wi}}$	$\frac{\phi}{1-\phi}$
Mirzaei-Paiaman et al. (2015)	$0.0314\sqrt{\frac{K}{\phi}}$	$0.0314\sqrt{K}$	$\sqrt{\phi}$

a-lithology factor, m-the cementation exponent (same definition with Archie law); Swi-irreducible (or connate) water saturation.

tribution in the pore space during drainage and imbibition processes. It depends strongly on petrophysical parameters, and fluid properties that may vary significantly throughout the reservoir. Variability of capillary pressure in reservoir determines the efficiency of waterflooding, hence, dominates the oil recovery and development program for Enhanced-Oil-Recovery (EOR) processes. Capillary pressure curve is often required for standard reservoir-simulation models accounting for the history dependence on initial and residual saturations. The capillary pressure curve is usually measured directly by injecting a non-wetting phase, such as mercury, in a rock sample saturated with wetting phase. However, due to environmental concerns associated with mercury, computational methods have been successfully applied to simulate mercury intrusion through network modeling (Oren et al., 1998), lattice Boltzmann methods (Ahrenholz et al., 2008; Ramstad et al., 2009), and morphology-based methods (Silin et al., 2011). Capillary pressure curve depends on the type of fluid invasion mechanism, i.e., drainage and imbibition. For dimensionless drainage capillary pressure curves, it has been proved experimentally that Leveretts J-function gives a good match for relatively homogeneous rocks at strongly water-wet conditions. However, for imbibition at mixed-wet conditions, J-function does not work satisfactorily since the permeability dependence on capillary pressure has been reported to be weak (Hamon and Pellerin, 1997; Hamon, 2000).

Recently, a semi-analytical model for imbibition process was proposed as an improved J-function to accurately describe the essential trends in capillary pressure behavior by Zhou et al. (2012), who used a simple 2D SEM image containing many separate, irregularly shaped pores at any capillary pressure and wetting condition by combining the free-energy minimization with arc meniscus (AM),

$$J(S_w) = \frac{P_c(S_w)}{\sigma \cos\theta_{eff}}\sqrt{\frac{K}{\phi}} \tag{11}$$

In above formulation, the contact angle θ was replaced by an effective contact angle $\cos\theta_{eff}$ given as:

$$\cos\theta^w_{eff} = \left(\frac{\sum_i L^w_{os,i}\cos\theta^w_{c,i} + L^w_{ow,i}}{\sum_i L^w_{os,i} + L^w_{ow,i}}\right)_{P_c=P_{c,max}} \tag{12}$$

$$\cos\theta^o_{eff} = \left(\frac{\sum_i L^o_{os,i}\cos\theta^o_{c,i} + L^o_{ow,i}}{\sum_i L^o_{os,i} + L^o_{ow,i}}\right)_{P_c=P_{c,max}} \tag{13}$$

$$\cos\theta_{eff} = \left|\cos\theta^w_{eff}\right| H(P_c) + \left|\cos\theta^o_{eff}\right| H(-P_c) \tag{14}$$

$$H(x) = \begin{cases} 1, & \text{if } x \geq 0 \\ 0, & \text{if } x < 0 \end{cases} \tag{15}$$

where, L_{os} and L_{ow} are the lengths of the oil-solid pore-boundary segments and arc meniscuses, respectively. The new dimensionless capillary pressure function and corresponding cross-sectional fluid configurations in these pore spaces were obtained.

In Zhou et al.'s model, by treating the pore spaces as cross sections of straight tubes, transient behavior was simulated, and initial conditions were established by drainage and wettability alteration. This operation is based on simplified assumptions that may lead to inaccurate results from the model. To address these limitations, Wang and Dong (2011) developed an interacting tube-bundle model with triangular tube cross sections in which both fluids can coexist at the same tube cross section, implying that the phase pressures vary with distance along the tube length, but remain constant in each cross section. Subsequently, the developed interacting tube-bundle model was used to simulate waterflooding to estimate effects of initial saturation and wettability on capillary-dominated water invasion using a SEM image (Zhou et al., 2014).

When the formation pressure of the reservoir falls below the bubblepoint pressure, the dissolved natural gas in the oil in the in-situ condition will liberate to form a three-phase flow with the injected water. Three phase flow conditions are also relevant in many other subsurface processes, including secondary oil recovery processes such as Water-Alternating-Gas (WAG) injection, and carbon dioxide (CO_2) injection for sequestration and/or EOR. Thus, these processes need a three-phase, mixed-wet capillary curve that is complexand needs further attention as compared to conventional two-phase capillary curves for oil/water, gas/water, or gas/oil. Virnovsky et al. (2004) tried to measure three-phase capillary pressure from core-plug, which was reported to be an extremely time-consuming and technically challenging task. Therefore, a simplified approach to this problem is to obtain empirically fitted correlations for three-phase capillary pressure and relative permeability through readily available two-phase data in reservoir simulation (Baker, 1988; Blunt, 1999). However, it has been proved that this method is not always practical at different wetting conditions (Egermann

et al., 2014). In addition to core-and pore-scale laboratory measurements, pore-scale simulations of multiphase flow can be used to propose correlations between capillary pressure and relative permeability. Recently, three-phase capillary pressure curves and fluid configurations at mixed-wet conditions were calculated by Zhou et al. (2015) based on the developed Mayer-Stowe-Princen method (Dijke et al., 2007). The results demonstrated that gas invades the oil-filled pores before the water-filled pores at water-wet conditions, and three-phase oil/water and gas/oil capillary pressure curves are functions of two saturations at mixed-wettability conditions. Pore geometry strongly affects the three-phase capillary pressure and related saturation paths in mixed-wet rock.

Significant progress has been made in simulating more complex processes with less information, however, there is still some room for improvements in current approach. Specifically, pore-connectivity effects, and consequently, phase trapping, residual saturations, and hysteresis have been disregarded in the straight tube-bundle models. Tortuous flow path with variably shaped apertures or with variable lengths have successfully been derived and applied in the flow properties characterization using fractal based approach (Cai and Yu, 2011; Cai et al., 2014a; Liu et al., 2016b). Thus, application of simple physical theory to simulate a capillary curve in a complex, irregular and disordered pore space is a missing requirement.

6. Conclusion and outlook

This review focuses on the applications of digital core analysis technology in petrophysical characterization, including the porous media imaging, characterization of petrophysical properties in 2D thin section, division of hydraulic flow units, and the construction of capillary curves. DRP technique is a relatively recent field of research in computational geosciences, besides other related areas of micro-tomography for petrophysics. Therefore, DRP is still developing and some challenges include: 1) large-scale digital core modeling technology. For instance, in practical applications, the size of the digital core is often required to be large enough (i.e., macro-scale) to reflect as many as possible heterogeneous structure to keep the stability of the calculated equivalent parameters and the comparability with the actual situation within the rocks. This requires that the resolution and size of the digital core have reached both a more refined level and a larger scale. Due to the physical constraints, however, the size and resolution of the established digital cores often cannot meet the requirement at the same time. The scale of volume simulated by DRP at present is about 1^3 cm^3, which is a practically negligible scale to study the processes occurring at field scale. Whether such a volume can represent the transmission, flow and mechanical behavior of the entire formation is questionable, but experience tells us that the laboratory scale cores always overestimate the recovery in comparison to its field scale observation. Therefore, it is safe to assume that simulation at such small scale as currently possible by DRP is not sufficient to describe the fluid flow behavior in the field. In this respect, an optimized scale-up method from the nanometer scale to the reservoir scale is a desirable goal. Some current approaches of scale-up include coupling the effective medium theory, computational homogenization, and percolation theory; 2) the determination of physical properties of digital core components, the rock matrix is not homogeneous and contains only a single component. Ideally, each pixel or pixel area needs to be assigned a different initial value in order to estimate more accurate results. However, the image series by μxCT scans only contains two phases, pores and solids without abundant mineral information. Therefore, all solid pixel values are assigned the same physical properties as the initial conditions to perform the simulation. This operation is a simplification process and it is necessary to obtain a database that reflects the distribution of 3D minerals to calculate Young's modulus and electric conductivity. We know that 2D thin sections are a slice of a 3D data body, implying that 2D thin sections can reflect the structure of the entire space to some extent. Therefore, by building a 2D-3D bridge, the petrophysical properties of 3D rocks can be estimated by converting the 2D properties using this "bridge". The high computational resource required for such simulations prevents many researchers to explore this field.

In conclusion, the uncertainties and challenges need to be highlighted in DRP. Significant progress is necessary to transform micro-tomography and conceptual model from the current research problem into a robust computational big data tool for multi-scale scientific and engineering problems in earth science related fields.

Acknowledgments

YZ acknowledges the support from The Royal Society International Exchanges Scheme-China (NSFC) Joint Project.

References

Aguilera, R. A method for estimating hydrocarbon cumulative production distribution of individual wells in naturally fractured carbonates, sandstones, shale gas, coalbed methane and tight gas formations. J. Can. Pet. Technol. 2010, 49(8): 53-58.

Aguilera, R. Flow units: from conventional to tight-gas to shale-gas to tight-oil to shale-oil reservoirs. SPE Reserv. Eval. Eng. 2014, 17(2): 190-208.

Ahrenholz, B., Tlke, J., Lehmann, P., et al. Prediction of capillary hysteresis in a porous material using lattice-Boltzmann methods and comparison to experimental data and a morphological pore network model. Adv. Water Resour. 2008, 31(9): 1151-1173.

Aliyev, E., Saidian, M., Prasad, M., et al. Rock typing of tight gas sands: A case study in Lance and Mesaverde formations from Jonah field. J. Nat. Gas Sci. Eng. 2016, 33: 1260-1270.

Amaefule, J.O., Altunbay, M., Tiab, D., et al. Enhanced reservoir description: Using core and log data to identify

hydraulic (flow) units and predict permeability in uncored intervals/wells. Paper SPE 26436 Presented at SPE Annual Technical Conference and Exhibition, Houston, Texas, 3-6 October, 1993.

Andr, H., Combaret, N., Dvorkin, J., et al. Digital rock physics benchmarkspart II: Computing effective properties. Comput. Geosci. 2013, 50: 33-43.

Archie, G.E. Introduction to petrophysics of reservoir rocks. AAPG Bull. 1950, 34(5): 943-961.

Arns, J.Y., Sheppard, A., Arns, C., et al. Pore-level validation of representative pore networks obtained from micro-CT images. Paper SCA2007-15 Presented at the International Symposium of the Society of Core Analysts held in Calgary, Canada, 10-12 September, 2007.

Asmussen, P., Conrad, O., Gnther, A., et al. Semi-automatic segmentation of petrographic thin section images using a "seeded-region growing algorithm"with an application to characterize wheathered subarkose sandstone. Comput. Geosci. 2015, 83: 89-99.

Baker, L.E. Three-phase relative permeability correlations. Paper SPE 17369 Presented at SPE Enhanced Oil Recovery Symposium, Tulsa, Oklahoma, 16-21 April, 1988.

Balhoff, M.T., Wheeler, M.F. A predictive pore-scale model for non-darcy flow in porous media. SPE J. 2009, 14(4): 579-587.

Baveye, P.C., Laba, M., Otten, W., et al. Observer-dependent variability of the thresholding step in the quantitative analysis of soil images and X-ray microtomography data. Geoderma 2010, 157(1-2): 51-63.

Behrang, A., Kantzas, A. A hybrid methodology to predict gas permeability in nanoscale organic materials; a combination of fractal theory, kinetic theory of gases and Boltzmann transport equation. Fuel 2017, 188: 239-245.

Blunt, M.J. An empirical model for three-phase relative permeability. SPE J. 1999, 5(4): 435-445.

Blunt, M.J., Bijeljic, B., Dong, H., et al. Pore-scale imaging and modelling. Adv. Water Resour. 2013, 51: 197-216.

Blunt, M.J., Jackson, M.D., Piri, M., et al. Detailed physics, predictive capabilities and macroscopic consequences for pore-network models of multiphase flow. Adv. Water Resour. 2002, 25(8): 1069-1089.

Borazjani, O., Ghiasi-Freez, J., Hatampour, A. Two intelligent pattern recognition models for automatic identification of textural and pore space characteristics of the carbonate reservoir rocks using thin section images. J. Nat. Gas Sci. Eng. 2016, 35: 944-955.

Byon, C., Kim, S.J. The effect of the particle size distribution and packing structure on the permeability of sintered porous wicks. Int. J. Heat Mass Transf. 2013, 61: 499-504.

Cai, J., Perfect, E., Cheng, C.L., et al. Generalized modeling of spontaneous imbibition based on Hagen-Poiseuille flow in tortuous capillaries with variably shaped apertures. Langmuir 2014a, 30(18): 5142-5151.

Cai, J., San José Martínez, F., Martín, M.A., et al. An introduction to flow and transport in fractal models of porous media: Part II. Fractals 2015, 23(1): 1502001.

Cai, J., San José Martiínez, F., Martín, M. A., et al. An introduction to flow and transport in fractal models of porous media: Part I. Fractals 2014b, 22(3): 1402001.

Cai, J., Yu, B. A discussion of the effect of tortuosity on the capillary imbibition in porous media. Transp. Porous Media 2011, 89(2): 251-263.

Cai, J., Yu, B., Zou, M., et al. Fractal analysis of invasion depth of extraneous fluids in porous media. Chem. Eng. Sci. 2010, 65(18): 5178-5186.

Chalmers, G.R., Bustin, R.M., Power, I.M. Characterization of gas shale pore systems by porosimetry, pycnometry, surface area, and field emission scanning electron microscopy/transmission electron microscopy image analyses: Examples from the barnett, woodford, haynesville, marcellus, and doig units. AAPG Bull. 2012, 96(6): 1099-1119.

Chen, S., Doolen, G.D. Lattice Boltzmann method for fluid flows. Annu. Rev. Fluid Mech. 1998, 30(1): 329-364.

Chen, X., Yao, G., Cai, J., et al. Fractal and multifractal analysis of different hydraulic flow units based on micro-CT images. J. Nat. Gas Sci. Eng. 2017, 48: 145-156.

Clarkson, C.R., Haghshenas, B., Ghanizadeh, A., et al. Nanopores to megafractures: Current challenges and methods for shale gas reservoir and hydraulic fracture characterization. J. Nat. Gas Sci. Eng. 2016, 31: 612-657.

Clarkson, C.R., Solano, N., Bustin, R.M., et al. Pore structure characterization of North American shale gas reservoirs using USANS/SANS, gas adsorption, and mercury intrusion. Fuel 2013, 103: 606-616.

Comunian, A., Renard, P., Straubhaar, J. 3D multiple-point statistics simulation using 2D training images. Comput. Geosci. 2012, 40: 49-65.

Deng, H., Hu, X., Li, H.A., et al. Improved pore-structure characterization in shale formations with FESEM technique. J. Nat. Gas Sci. Eng. 2016, 35: 309-319.

Desbois, G., Urai, J.L., Kukla, P.A., et al. High-resolution 3D fabric and porosity model in a tight gas sandstone reservoir: A new approach to investigate microstructures from mm- to nm-scale combining argon beam cross-sectioning and SEM imaging. J. Pet. Sci. Eng. 2011, 78(2): 243-257.

Dijke, M.I.J.V., Piri, M., Helland, J.O., et al. Criteria for three-fluid configurations including layers in a pore with nonuniform wettability. Water Resour. Res. 2007, 43(12): 55-60.

Dong, H., Blunt, M.J. Pore-network extraction from micro-computerized-tomography images. Phys. Rev. E 2009, 80(3): 036307.

Dvorkin, J., Derzhi, N., Diaz, E., et al. Relevance of computational rock physics. Geophysics 2011, 76(5): E141-E153.

Egermann, P., Mejdoub, K., Lombard, J.M., et al. Drainage three-phase flow relative permeability on oil-wet carbonate reservoir rock types: Experiments, interpretation and comparison with standard correlations. Petrophysics 2014, 55(4): 287-293.

Fu, H., Tang, D., Xu, T., et al. Characteristics of pore structure and fractal dimension of low-rank coal: A case study of Lower Jurassic Xishanyao coal in the southern Junggar Basin, NW China. Fuel 2017, 193: 254-264.

Ge, X., Fan, Y., Li, J., et al. Pore structure characterization and classification using multifractal theory−An application in Santanghu basin of western China. J. Pet. Sci. Eng. 2015, 127: 297-304.

Gundogar, A.S., Ross, C.M., Akin, S., et al. Multiscale pore structure characterization of middle east carbonates. J. Pet. Sci. Eng. 2016, 146: 570-583.

Hajizadeh, A., Safekordi, A., Farhadpour, F.A. A multiple-point statistics algorithm for 3D pore space reconstruction from 2D images. Adv. Water Resour. 2011, 34(10): 1256-1267.

Hamon, G. Field-wide variations of wettability. Paper SPE 63144 Presented at SPE Annual Technical Conference and Exhibition, Texas, 1-4 October, 2000.

Hamon, G., Pellerin, F. Evidencing capillary pressure and relative permeability trends for reservoir simulation. Paper SPE 38898 Presented at SPE Annual Technical Conference and Exhibition, San Antonio, Texas, 5-8 October, 1997.

Helland, J.O., Zhou, Y., Hatzignatiou, D.G. Dynamic capillary pressure curves from pore-scale modeling in mixed-wet-rock images. SPE J. 2013, 18(4): 634-645.

Hikosaka, R., Nagata, F., Tomita, M., et al. Optimization of pore structure and particle morphology of mesoporous silica for antibody adsorption for use in affinity chromatography. Appl. Surf. Sci. 2016, 384: 27-35.

Hildebrand, T., Ruegsegger, P. A new method for the model-independent assessment of thickness in three-dimensional images. J. Microsc. 1997, 185: 67-75.

Hinai, A.A., Rezaee, R., Esteban, L., et al. Comparisons of pore size distribution: A case from the Western Australian gas shale formations. J. Unconv. Oil Gas Resour. 2014, 8: 1-13.

Hofmann, P., Marschallinger, R., Unterwurzacher, M., et al. Marble provenance designation with object based image analysis: State-of-the-art rock fabric characterization from petrographic micrographs. Austrian J. Earth Sci. 2013, 106(2): 73-82.

Houston, A.N., Otten, W., Baveye, P.C., et al. Adaptive-window indicator kriging: A thresholding method for computed tomography images of porous media. Comput. Geosci. 2013a, 542: 39-48.

Houston, A.N., Schmidt, S., Tarquis, A.M., et al. Effect of scanning and image reconstruction settings in X-ray computed microtomography on quality and segmentation of 3D soil images. Geoderma 2013b, 208: 154-165.

Iassonov, P., Gebrenegus, T., Tuller, M. Segmentation of X-ray computed tomography images of porous materials: A crucial step for characterization and quantitative analysis of pore structures. Water Resour. Res. 2009, 45(9): W09415.

Ismail, I., Gamio, J.C., Bukhari, S.F.A., et al. Tomography for multi-phase flow measurement in the oil industry. Flow Meas. Instrum. 2005, 16(2-3): 145-155.

Izadi, H., Baniassadi, M., Hasanabadi, A., et al. Application of full set of two point correlation functions from a pair of 2D cut sections for 3D porous media reconstruction. J. Pet. Sci. Eng. 2017a, 149: 789-800.

Izadi, H., Sadri, J., Bayati, M. An intelligent system for mineral identification in thin sections based on a cascade approach. Comput. Geosci. 2017b, 99: 37-49.

Izadi, H., Sadri, J., Mehran, N.A. A new intelligent method for minerals segmentation in thin sections based on a novel incremental color clustering. Comput. Geosci. 2015, 81: 38-52.

Kareem, R., Cubillas, P., Gluyas, J., et al. Multi-technique approach to the petrophysical characterization of Berea sandstone core plugs (Cleveland Quarries, USA). J. Pet. Sci. Eng. 2017, 149: 436-455.

Keehm, Y., Mukerji, T., Nur, A. Permeability prediction from thin sections: 3D reconstruction and Lattice−Boltzmann flow simulation. Geophys. Res. Lett. 2004, 31: L04606.

Khoei, A., Hosseini, N., Mohammadnejad, T. Numerical modeling of two-phase fluid flow in deformable fractured porous media using the extended finite element method and an equivalent continuum model. Adv. Water Resour. 2016, 94: 510-528.

Landry, C.J., Karpyn, Z.T., Ayala, O. Relative permeability of homogenous-wet and mixed-wet porous media as determined by pore-scale lattice Boltzmann modeling. Water Resour. Res. 2014, 50(5): 3672-3689.

Lemmens, H., Butcher, A., Botha, P.W. FIB/SEM and automated mineralogy for core and cuttings analysis. Paper SPE 136327 Presented at the SPE Russian oil and gas conference and exhibition, Moscow, Russia 26-28 October, 2010,

Li, Z., Favier, J., D'Ortona, U., et al. An immersed boundary-lattice Boltzmann method for single- and multi-component fluid flows. J. Comput. Phys. 2016, 304(C): 424-440.

Liang, Z., Ioannidis, M., Chatzis, I. Permeability and electrical conductivity of porous media from 3D stochastic replicas of the microstructure. Chem. Eng. Sci. 2000, 55(22): 5247-5262.

Liu, J., Pereira, G.G., Liu, Q., et al. Computational challenges in the analyses of petrophysics using microtomography and upscaling: A review. Comput. Geosci. 2016a, 89: 107-117.

Liu, R., Jiang, Y., Li, B., et al. A fractal model for characterizing fluid flow in fractured rock masses based on randomly distributed rock fracture networks. Comput. Geotech. 2015, 65: 45-55.

Liu, R., Jiang, Y., Li, B., et al. Estimating permeability of porous media based on modified Hagen-Poiseuille flow in tortuous capillaries with variable lengths. Microfluid. Nanofluid. 2016b, 20(8): 120.

Lopez, X., Valvatne, P.H., Blunt, M.J. Predictive network modeling of single-phase non-Newtonian flow in porous media. J. Colloid Interface Sci. 2003, 264(1): 256-265.

Madonna, C., Almqvist, B.S., Saenger, E.H. Digital rock physics: numerical prediction of pressure-dependent ultrasonic velocities using micro-CT imaging. Geophys.

J. Int. 2012, 189(3): 1475-1482.

Malpica, N., Ortiz de Solorzano, C., Vaquero, J.J., et al. Applying watershed algorithms to the segmentation of clustered nuclei. Cytometry 1997, 28(4): 289-297.

Marmo, R., Amodio, S., Tagliaferri, R., et al. Textural identification of carbonate rocks by image processing and neural network: Methodology proposal and examples. Comput. Geosci. 2005, 31(5): 649-659.

Martys, N.S., Chen, H.D. Simulation of multicomponent fluids in complex three-dimensional geometries by the lattice Boltzmann method. Phys. Rev. E 1996, 53(1): 743-750.

Meakin, P. Fractals, scaling and growth far from equilibrium. Cambridge, USA, Cambridge University Press, 1998.

Mirzaei-Paiaman, A., Saboorian-Jooybari, H. A method based on spontaneous imbibition for characterization of pore structure: Application in pre-SCAL sample selection and rock typing. J. Nat. Gas Sci. Eng. 2016, 35A: 814-825.

Mynarczuk, M. Description and classification of rock surfaces by means of laser profilometry and mathematical morphology. Int. J. Rock Mech. Min. 2010, 47(1): 138-149.

Mynarczuk, M., Grszczyk, A., lipek, B. The application of pattern recognition in the automatic classification of microscopic rock images. Comput. Geosci. 2013, 60: 126-133.

Mollajan, A., Ghiasi-Freez, J., Memarian, H. Improving pore type identification from thin section images using an integrated fuzzy fusion of multiple classifiers. J. Nat. Gas Sci. Eng. 2016, 31: 396-404.

Naraghi, M.E., Javadpour, F. A stochastic permeability model for the shale-gas systems. Int. J. Coal Geol. 2015, 140: 111-124.

Nie, B., Liu, X., Yang, L., et al. Pore structure characterization of different rank coals using gas adsorption and scanning electron microscopy. Fuel 2015, 158: 908-917.

Oh, W., Lindquist, B. Image thresholding by indicator kriging. IEEE Trans. Pattern Anal. Mach. Intell. 1999, 21(7): 590-602.

Okabe, H., Blunt, M.J. Pore space reconstruction using multiple-point statistics. J. Pet. Sci. Eng. 2005, 46(1-2): 121-137.

Oren, P.E., Bakke, S., Arntzen, O.J. Extending predictive capabilities to network models. SPE J. 1998, 3(4): 324-336.

Otsu, N. A threshold selection method from gray-level histograms. Automatica 1975, 11(285-296): 23-27.

Ougier-Simonin, A., Renard, F., Boehm, C., et al. Microfracturing and microporosity in shales. Earth-Sci. Rev. 2016, 162: 198-226.

Pan, N. Analytical characterization of the anisotropy and local heterogeneity of short fiber composites: Fiber fraction as a variable. J. Compos. Mater. 1994, 28(16): 1500-1531.

Peng, S., Hassan, A., Loucks, R.G. Permeability estimation based on thin-section image analysis and 2D flow modeling in grain-dominated carbonates. Mar. Pet. Geol. 2016, 77: 763-775.

Peng, S., Yang, J., Xiao, X., et al. An integrated method for upscaling pore-network characterization and permeability estimation: Example from the mississippian barnett shale. Transp. Porous Media 2015, 109(2): 359-376.

Raabe, D. Overview of the lattice Boltzmann method for nano- and microscale fluid dynamics in materials science and engineering. Model. Simul. Mat. Sci. Eng. 2004, 12(6): R13.

Rabbani, A., Ayatollahi, S., Kharrat, R., et al. Estimation of 3-D pore network coordination number of rocks from watershed segmentation of a single 2-D image. Adv. Water Resour. 2016, 94: 264-277.

Rabbani, A., Jamshidi, S. Specific surface and porosity relationship for sandstones for prediction of permeability. Int. J. Rock Mech. Min. 2014, 71: 25-32.

Rabbani, A., Jamshidi, S., Salehi, S. An automated simple algorithm for realistic pore network extraction from micro-tomography images. J. Pet. Sci. Eng. 2014a, 123: 164-171.

Rabbani, A., Jamshidi, S., Salehi, S. Determination of specific surface of rock grains by 2D imaging. J. Geol. Res. 2014b, 20: 141-147.

Ramstad, T., Oren, P.E., Bakke, S. Simulation of two phase flow in reservoir rocks using a lattice Boltzmann method. SPE J. 2009, 15(4): 917-927.

Ross, B., Fueten, F., Yashkir, D. Automatic mineral identification using genetic programming. Mach. Vision Appl. 2001, 13: 61-69.

Ryazanov, A.V., Dijke, M.I.J.V., Sorbie, K.S. Two-phase pore-network modelling: Existence of oil layers during water invasion. Transp. Porous Media 2009, 80(1): 79-99.

Sachsenhofer, R.F., Koltun, Y.V. Black shales in Ukraine-A review. Mar. Pet. Geol. 2012, 31(1): 125-136.

Sander, R., Pan, Z., Connell, L.D. Laboratory measurement of low permeability unconventional gas reservoir rocks: A review of experimental methods. J. Nat. Gas Sci. Eng. 2017, 37: 248-279.

Saxena, N., Mavko, G. Estimating elastic moduli of rocks from thin sections: Digital rock study of 3D properties from 2D images. Comput. Geosci. 2016, 889-921.

Saxena, N., Mavko, G., Hofmann, R., et al. Estimating permeability from thin sections without reconstruction: Digital rock study of 3D properties from 2D images. Comput. Geosci. 2017, 10: 279-299.

Sezgin, M. Survey over image thresholding techniques and quantitative performance evaluation. J. Electron. Imaging 2004, 13(1): 146-168.

Shan, X., Chen, H. Lattice Boltzmann model for simulating flows with multiple phases and components. Phys. Rev. E 1993, 47(3): 18-15.

Silin, D., Patzek, T. Pore space morphology analysis using maximal inscribed spheres. Phys. A 2006, 371(2): 336-360.

Silin, D., Tomutsa, L., Benson, S.M., et al. Microtomography and pore-scale modeling of two-phase fluid distribution. Transp. Porous Media 2011, 86(2): 495-515.

Singh, N., Singh, T., Tiwary, A., et al. Textural identification of basaltic rock mass using image processing and neural network. Comput. Geosci. 2010, 14(2): 301-310.

Song, W., Yao, J., Li, Y., et al. New pore size distribution calculation model based on chord length and digital image. J. Nat. Gas Sci. Eng. 2016.

Thompson, S., Fueten, F., Bockus, D. Mineral identification using artificial neural networks and the rotating polarizer stage. Comput. Geosci. 2001, 27(9): 1081-1089.

Tomutsa, L., Silin, D.B., Radmilovic, V. Analysis of chalk petrophysical properties by means of submicron-scale pore imaging and modeling. SPE Reserv. Eval. Eng. 2007, 10(3): 285-293.

Van den Berg, E., Meesters, A., Kenter, J., et al. Automated separation of touching grains in digital images of thin sections. Comput. Geosci. 2002, 28(2): 179-190.

Verma, A., Pitchumani, R. Fractal description of microstructures and properties of dynamically evolving porous media. Int. Commun. Heat Mass Transf. 2017, 81: 51-55.

Vidal, D., Ridgway, C., Pianet, G., et al. Effect of particle size distribution and packing compression on fluid permeability as predicted by lattice-Boltzmann simulations. Comput. Chem. Eng. 2009, 33(1): 256-266.

Virnovsky, G., Vatne, K., Iversen, J., et al. Three-phase capillary pressure measurements in centrifuge at reservoir conditions. Paper SCA2004-19 Presented at the International Symposium of the Society of Core Analysts, Abu Dhabi, 2004.

Wang, J., Dong, M. Trapping of the non-wetting phase in an interacting triangular tube bundle model. Chem. Eng. Sci. 2011, 66(3): 250-259.

Wang, J., Li, C., Kang, Q., et al. The lattice Boltzmann method for isothermal micro-gaseous flow and its application in shale gas flow: A review. Int. J. Heat Mass Transf. 2016a, 95: 94-108.

Wang, J., Zhao, J., Zhang, Y., et al. Analysis of the effect of particle size on permeability in hydrate-bearing porous media using pore network models combined with CT. Fuel 2016b, 163: 34-40.

Wang, M., Pan, N. Predictions of effective physical properties of complex multiphase materials. Mat. Sci. Eng. R Rep. 2008, 63(1): 1-30.

Wang, M., Wang, J., Pan, N., et al. Mesoscopic predictions of the effective thermal conductivity for microscale random porous media. Phys. Rev. E 2007, 75(3): 036702.

Wang, W., Kravchenko, A.N., Smucker, A.J.M., et al. Comparison of image segmentation methods in simulated 2D and 3D microtomographic images of soil aggregates. Geoderma 2011, 162(3-4): 231-241.

Wargo, E.A., Kotaka, T., Tabuchi, Y., et al. Comparison of focused ion beam versus nano-scale X-ray computed tomography for resolving 3-D microstructures of porous fuel cell materials. J. Power Sources 2013, 241: 608-618.

Wiegmann, A. Computation of the permeability of porous materials from their microstructure by FFF-Stokes. Fraunhofer-Institut fur Techno-und Wirtschaftsmathematik, Fraunhofer (ITWM), 2007.

Wiegmann, A., Bube, K.P. The explicit-jump immersed interface method: Finite difference methods for DEs with piecewise smooth aolutions. SIAM J. Numer. Anal. 2000, 37(3): 827-862.

Wilson, M.J., Wilson, L., Shaldybin, M.V. Clay mineralogy and unconventional hydrocarbon shale reservoirs in the USA. II. Implications of predominantly illitic clays on the physico-chemical properties of shales. Earth-Sci. Rev. 2016, 15: 81-88.

Wolfram, S. A New Kind of Science. Champaign, Wolfram media, 2002.

Xiao, D., Lu, S., Lu, Z., et al. Combining nuclear magnetic resonance and rate-controlled porosimetry to probe the pore-throat structure of tight sandstones. Pet. Exprol. Dev. 2016, 43(6): 1049-1059.

Xie, S., Cheng, Q., Ling, Q., et al. Fractal and multifractal analysis of carbonate pore-scale digital images of petroleum reservoirs. Mar. Pet. Geol. 2010, 27(2): 476-485.

Xu, P., Yu, B. Developing a new form of permeability and Kozeny−Carman constant for homogeneous porous media by means of fractal geometry. Adv. Water Resour. 2008, 31(1): 74-81.

Xu, Z., Teng, Q., He, X., et al. Multiple-point statistics method based on array structure for 3D reconstruction of Fontainebleau sandstone. J. Pet. Sci. Eng. 2012, 100: 71-80.

Yan, Y.Y., Zu, Y.Q., Dong, B. LBM, a useful tool for mesoscale modelling of single-phase and multiphase flow. Appl. Therm. Eng. 2011, 31(5): 649-655.

Yang, C., Zhang, J., Tang, X., et al. Comparative study on micro-pore structure of marine, terrestrial, and transitional shales in key areas, China. Int. J. Coal Geol. 2017, 171: 76-92.

Yiotis, A.G., Tsimpanogiannis, I.N., Stubos, A.K., et al. Pore-network study of the characteristic periods in the drying of porous materials. J. Colloid Interface Sci. 2006, 297(2): 738-748.

Young, I., Crawford, J., Rappoldt, C. New methods and models for characterising structural heterogeneity of soil. Soil Tillage Res. 2001, 61(1): 33-45.

Yu, B., Cheng, P. A fractal permeability model for bi-dispersed porous media. Int. J. Heat Mass Transf. 2002, 45(14): 2983-2993.

Yu, B., Cheng, P., Zhan, X., et al. Pore-scale modeling of electrical and fluid transport in Berea sandstone. Geophyscics 2010, 75(75): F135-F142.

Zhao, Y., Sun, Y., Liu, S., et al. Pore structure characterization of coal by NMR cryoporometry. Fuel 2017, 190: 359-369.

Zhou, Y., Helland, J., Hatzignatiou, D.G. Pore-scale modeling of waterflooding in mixed-wet-rock images: Effects of initial saturation and wettability. SPE J. 2014, 19(1): 88-100.

Zhou, Y., Helland, J.O., Hatzignatiou, D.A. Dimensionless capillary pressure function for imbibition derived from pore-scale modelling in mixed-wet rock images. SPE J. 2012, 18(2): 296-308.

Zhou, Y., Helland, J.O., Hatzignatiou, D.G. Computation of three-phase capillary pressure curves and fluid configurations at mixed-wet conditions in 2D rock images. SPE J. 2016, 21(1): 152-169.